J. Fluid Mech. (1995), *vol.* 286, *pp.* 229–255

A dynamic localization model for large-eddy simulation of turbulent flows

By SANDIP GHOSAL, THOMAS S. LUND, PARVIZ MOIN AND KNUT AKSELVOLL

Center for Turbulence Research, Stanford University, Stanford, CA 94305, USA

(Received 17 June 1994 and in revised form 3 October 1994)

In a previous paper, Germano, *et al.* (1991) proposed a method for computing coefficients of subgrid-scale eddy viscosity models as a function of space and time. This procedure has the distinct advantage of being self-calibrating and requires no *a priori* specification of model coefficients or the use of wall damping functions. However, the original formulation contained some mathematical inconsistencies that limited the utility of the model. In particular, the applicability of the model was restricted to flows that are statistically homogeneous in at least one direction. These inconsistencies and limitations are discussed and a new formulation that rectifies them is proposed. The new formulation leads to an integral equation whose solution yields the model coefficient as a function of position and time. The method can be applied to general inhomogeneous flows and does not suffer from the mathematical inconsistencies inherent in the previous formulation. The model has been tested in isotropic turbulence and in the flow over a backward-facing step.

1. Introduction

In large-eddy simulation (LES) one needs to model the subgrid-scale stress tensor $\tau_{ij} = \overline{u_i u_j} - \overline{u}_i \overline{u}_j$, where the bar denotes some local average (filter) that removes the high spatial frequencies. One popular eddy viscosity model (Smagorinsky 1963) is

$$\tau_{ij} - \tfrac{1}{3}\delta_{ij}\tau_{kk} = -2C\Delta^2|\overline{S}|\overline{S}_{ij}. \tag{1.1}$$

Here Δ is the filter width, $\overline{S}_{ij}$ is the strain rate tensor defined as

$$\overline{S}_{ij} = \frac{1}{2}\left(\frac{\partial \overline{u}_i}{\partial x_j} + \frac{\partial \overline{u}_j}{\partial x_i}\right), \tag{1.2}$$

C is a dimensionless parameter and $|\overline{S}| = (2\overline{S}_{ij}\overline{S}_{ij})^{1/2}$.

The dynamic model (Germano *et al.* 1991) is a method for computing C at each time-step as a function of position from the information already contained in the resolved velocity field (rather than treating it as an adjustable parameter). There are two advantages to this. Firstly, it gives a systematic procedure for computing a flow about which there is no prior experience and therefore no guidance is available to adjust the parameter C. Secondly, in an inhomogeneous flow, the optimum choice of C may be a function of position; one does not expect the entire flow to be represented by a single constant. The same consideration applies to flows undergoing transition to turbulence or more generally, to flows whose statistical properties are changing with time. In the traditional approach, one needs to introduce further arbitrary

assumptions, such as wall damping functions or a prescription to reset the value of C from zero to a finite number as the flow undergoes transition to turbulence. In contrast, inhomogeneous and statistically unsteady flows can be handled very naturally in the context of the dynamic model since C is a function of position and time. Though the dynamic model lacked the full generality necessary to handle general turbulent flows with no homogeneous directions, the method had some important successes (Piomelli 1993; Cabot & Moin 1993; Moin *et al.* 1991; Zang, Street & Koseff 1993; Bohnert & Ferziger 1993).

The basic formalism behind the method proposed by Germano *et al.* (1991) is summarized below. To compute C one first introduces a 'test' filtering operation on the large-eddy field that is denoted by the symbol ' $\widehat{\ }$ ':

$$\widehat{\psi}(\boldsymbol{x}) = \int G(\boldsymbol{x}, \boldsymbol{y})\psi(\boldsymbol{y})\mathrm{d}\boldsymbol{y}, \tag{1.3}$$

where $G(\boldsymbol{x}, \boldsymbol{y})$ is any kernel that serves to damp spatial fluctuations shorter than some characteristic length $\widehat{\Delta} > \Delta$ and $\boldsymbol{x}$, $\boldsymbol{y}$ are position vectors. The equations for the test-filtered field contain the 'test-level' subgrid-scale stress term

$$T_{ij} = \widehat{\overline{u_i}\overline{u_j}} - \widehat{\overline{u}}_i\widehat{\overline{u}}_j. \tag{1.4}$$

Both T_{ij} and τ_{ij} are unknown in LES; however, the two tensors are related by the identity (Germano *et al.* 1991)

$$L_{ij} = T_{ij} - \widehat{\tau}_{ij}. \tag{1.5}$$

Here the Leonard term $L_{ij} = \widehat{\overline{u_i}\overline{u_j}} - \widehat{\overline{u}}_i\widehat{\overline{u}}_j$ is computable from the large-eddy field. Finally, it is assumed that a scaling law is operative and therefore the subgrid-scale stress at the test level may be written as

$$T_{ij} - \tfrac{1}{3}\delta_{ij}T_{kk} = -2C\widehat{\Delta}^2|\widehat{\overline{S}}|\widehat{\overline{S}}_{ij}. \tag{1.6}$$

On substituting (1.1) and (1.6) into (1.5) an equation for determining C is obtained:

$$L_{ij} - \tfrac{1}{3}\delta_{ij}L_{kk} = \alpha_{ij}C - \widehat{\beta_{ij}C} \tag{1.7}$$

where

$$\alpha_{ij} = -2\widehat{\Delta}^2|\widehat{\overline{S}}|\widehat{\overline{S}}_{ij}, \tag{1.8}$$

$$\beta_{ij} = -2\Delta^2|\overline{S}|\overline{S}_{ij}. \tag{1.9}$$

The method of obtaining C from (1.7) used by previous authors contained some mathematical inconsistencies which are discussed in the next section. Moreover, the expression for C so derived resulted in the simulation becoming unstable. To avoid the instability a prescription of averaging over homogeneous directions was adopted which could not be justified except in a heuristic way. A more serious limitation was that the prescription would not work in flows that have no homogeneous directions. Admittedly *ad hoc* schemes could still be found to make the method 'work' in inhomogeneous flows. Prescriptions such as a local 'smoothing' by averaging over neighbouring grid cells with or without 'clipping' (setting negative values of C to zero) have been used in inhomogeneous flows and reasonable agreement with experiments have been achieved (see e.g. Zang *et al.* 1993). In this paper our aim is to develop a method of computing C using (1.7) in a mathematically consistent fashion without resorting to arbitrary prescriptions. In the process of doing so we demonstrate that some of the expressions for C used by previous authors that appeared to be without

formal justification can in fact be derived rigorously starting from a few clearly stated assumptions. The principal goal of this work is to put the dynamic modelling procedure on firm theoretical foundations so that the method can be applied to arbitrary inhomogeneous flows without recourse to *ad hoc* procedures.

1.1. *Difficulties with previous models*

Since C appears inside the filtering operation, (1.7) is a system of five (since the tensors are symmetric and traceless) independent integral equations involving only one function C. In previous formulations (Germano *et al.* 1991; Moin *et al.* 1991; Lilly 1992) one simply ignored the fact that C is a function of position and took C out of the filtering operation as if it were a constant. This rather arbitrary procedure cannot be justified *a posteriori* because the C field computed using this procedure is found to be a rapidly varying function of position (Moin 1991). Nevertheless, the procedure reduced the system of integral equations to algebraic equations at each point of the field. The redundancy of equations is dealt with (Lilly 1992) by choosing C to 'best satisfy' all the equations, that is, C is chosen so as to minimize the sum of the squares of the residuals $E_{ij}(\boldsymbol{x})E_{ij}(\boldsymbol{x})$ where

$$E_{ij} = L_{ij} - \tfrac{1}{3}\delta_{ij}L_{kk} - \alpha_{ij}C + \widehat{\beta}_{ij}C. \tag{1.10}$$

The result is

$$C = \frac{m_{ij}L_{ij}}{m_{kl}m_{kl}} \tag{1.11}$$

where $m_{ij} = \alpha_{ij} - \widehat{\beta}_{ij}$. (Throughout this paper summation over repeated indices is implied.)

The C obtained from (1.11) can be either positive or negative. A negative value of C implies a locally negative eddy viscosity, which in turn implies a flow of energy from the small scales to the resolved scales or backscatter. It is known from direct numerical simulation (DNS) data (Piomelli *et al.* 1991) that the forward and reverse cascades of energy in a turbulent flow are typically of the same order of magnitude with a slight excess of the former accounting for the overall transfer of energy from large to small scales. The presence of backscatter therefore is a desirable feature of a subgrid-scale model. However, when (1.11) is used in an LES the computation is found to become unstable. The instability can be traced to the fact that C has a large auto-correlation time. Therefore, once it becomes negative in some region, it may remain negative for excessively long periods of time during which the exponential growth of the local velocity fields, associated with negative eddy viscosity, causes a divergence of the total energy (Lund, Ghosal & Moin 1993). Though this issue of stability remained unresolved, a way around the problem was found if the flow possessed at least one homogeneous direction. One assumed C to be independent of the homogeneous directions and to make (1.11) consistent with this assumption, the numerator and denominator were averaged over the homogeneous directions. The averaging made C a more smoothly varying function that rarely became negative. This scheme has produced results in very good agreement with experiments and DNS (Germano *et al.* 1991; Moin *et al.* 1991; Cabot & Moin 1993). The disadvantages are: (*a*) it is based on an *ad hoc* procedure; (*b*) the prescription can only be applied to flows that have at least one homogeneous direction, thus excluding the more challenging flows of engineering interest.

In the next section we give a formulation that removes the inconsistency involved in reducing the integral equations (1.7) to algebraic equations. In §3 we derive the

spatial averaging prescription of Germano *et al.* (1991) within the general framework of this new formulation for flows having homogeneous directions and show how to generalize the method to inhomogeneous flows. We call this new model the *dynamic localization model (constrained)* to stress the fact that the coefficient field C is a function of all three coordinates as well as time but is restricted to have non-negative values. In §4 the model is extended to allow for backscatter with the inclusion of an equation for the subgrid kinetic energy budget. The new model, which we will refer to as the *dynamic localization model (k-equation)*, is evaluated from the point of view of stability, realizability, Galilean invariance and behaviour near solid walls. Some issues of numerical implementation are addressed in §5. In §6 the dynamic localization model (constrained) is applied to the problem of turbulent flow over a backward-facing step as an example of a complex geometry flow. Some tests on isotropic turbulence are also summarized. Conclusions are presented in §7.

2. A variational formulation

The mathematical inconsistency associated with removing the 'C' from the filtering operation discussed in the last section can be removed by the following generalization of the least-square minimization procedure. The 'error' in satisfying (1.7) for a given coefficient field C is

$$E_{ij}(\boldsymbol{x}) = L_{ij} - \tfrac{1}{3}\delta_{ij}L_{kk} - \alpha_{ij}C + \widehat{\beta_{ij}C}. \tag{2.1}$$

At any given point, '$\boldsymbol{x}$', E_{ij} depends on the value of the function C at neighbouring points in the field. One cannot therefore minimize the sum of the squares of the residuals $E_{ij}E_{ij}$ locally since reducing the value of $E_{ij}E_{ij}$ at one point changes its values at neighbouring points. However, the method of least squares has a natural generalization to the non-local case. The function C that 'best satisfies' the integral equations (1.7) is the one that minimizes

$$\mathscr{F}[C] = \int E_{ij}(\boldsymbol{x})E_{ij}(\boldsymbol{x})\mathrm{d}\boldsymbol{x}. \tag{2.2}$$

$\mathscr{F}[C]$ is a functional of C and the integral extends over the entire domain. To find the Euler–Lagrange equation for this minimization problem, we set the variation of $\mathscr{F}$ to zero:

$$\delta\mathscr{F} = 2\int E_{ij}(\boldsymbol{x})\delta E_{ij}(\boldsymbol{x})\mathrm{d}\boldsymbol{x} = 0. \tag{2.3}$$

Using the definition of E_{ij} we get

$$\int \left(-\alpha_{ij}E_{ij}\delta C + E_{ij}\widehat{\beta_{ij}\delta C}\right)\mathrm{d}\boldsymbol{x} = 0 \tag{2.4}$$

which may be rearranged as

$$\int \left(-\alpha_{ij}E_{ij} + \beta_{ij}\int E_{ij}(\boldsymbol{y})G(\boldsymbol{y},\boldsymbol{x})\mathrm{d}\boldsymbol{y}\right)\delta C(\boldsymbol{x})\mathrm{d}\boldsymbol{x} = 0. \tag{2.5}$$

Thus, the Euler–Lagrange equation is

$$-\alpha_{ij}E_{ij} + \beta_{ij}\int E_{ij}(\boldsymbol{y})G(\boldsymbol{y},\boldsymbol{x})\mathrm{d}\boldsymbol{y} = 0 \tag{2.6}$$

which may be rewritten in terms of C as

$$f(x) = C(x) - \int \mathscr{K}(x,y)C(y)\mathrm{d}y \tag{2.7}$$

where

$$f(x) = \frac{1}{\alpha_{kl}(x)\alpha_{kl}(x)}\left[\alpha_{ij}(x)L_{ij}(x) - \beta_{ij}(x)\int L_{ij}(y)G(y,x)\mathrm{d}y\right],$$

$$\mathscr{K}(x,y) = \frac{\mathscr{K}_{\mathscr{A}}(x,y) + \mathscr{K}_{\mathscr{A}}(y,x) - \mathscr{K}_{\mathscr{S}}(x,y)}{\alpha_{kl}(x)\alpha_{kl}(x)}$$

and

$$\mathscr{K}_{\mathscr{A}}(x,y) = \alpha_{ij}(x)\beta_{ij}(y)G(x,y),$$

$$\mathscr{K}_{\mathscr{S}}(x,y) = \beta_{ij}(x)\beta_{ij}(y)\int \mathrm{d}z\, G(z,x)G(z,y).$$

Equation (2.7) is readily recognized as Fredholm's integral equation of the second kind. Under certain conditions it admits a unique solution.

Even though this formulation removes the inconsistency associated with taking C out of the '$\hat{}$' operator, it does not remove the instability associated with negative eddy viscosity. In the following sections we show two methods that address this stability problem.

3. The constrained variational formulation

In this section we address the stability problem created by the negative eddy viscosity by requiring that in addition to minimizing the functional in (2.2), C satisfies some constraints designed to ensure the stability of the model. The choice of such constraints is clearly not unique and different models may be constructed by changing the constraint. Thus, it will be shown that the local least-squares method (Lilly 1992) coupled with the volume-averaging prescription (Germano *et al.* 1991) can actually be derived as a rigorous consequence of such a constrained variational problem for flows with at least one homogeneous direction. The method is then extended to general inhomogeneous flows by imposing a constraint that does not rely on the existence of homogeneous directions. All of these methods are designed to prevent instability in the calculations by ruling out backscatter in one way or another. This restriction is removed in §4 where the theory presented in this section is extended to allow for backscatter without causing an instability.

3.1. *Homogeneous turbulence*

In the case of homogeneous turbulence, it is natural to assume that C can depend only on time (note that the eddy viscosity $\nu_t = C\Delta^2|\bar{S}|$ is still a function of space as well as time). Let us therefore impose this as a constraint in the problem of minimizing the functional (2.2). The functional $\mathscr{F}[C]$ then reduces to the function

$$\mathscr{F}(C) = \langle \mathscr{L}_{ij}\mathscr{L}_{ij}\rangle - 2\langle \mathscr{L}_{ij}m_{ij}\rangle C + \langle m_{ij}m_{ij}\rangle C^2 \tag{3.1}$$

where $\mathscr{L}_{ij} = L_{ij} - (1/3)\delta_{ij}L_{kk}$ is the anisotropic part of L_{ij}, $m_{ij} = \alpha_{ij} - \widehat{\beta}_{ij}$ and $\langle\ \rangle$

denotes integral over the volume. The value of C that minimizes the function $\mathscr{F}(C)$ is easily found to be

$$C = \frac{\langle m_{ij}\mathscr{L}_{ij}\rangle}{\langle m_{kl}m_{kl}\rangle} = \frac{\langle m_{ij}L_{ij}\rangle}{\langle m_{kl}m_{kl}\rangle}. \tag{3.2}$$

The latter equality holds since m_{ij} is traceless. Equation (3.2) is precisely the result of Lilly. In the rest of this paper we will refer to expression (3.2) and its counterpart for partially homogeneous flows (3.6) as the *dynamic model.*

3.2. *Flows with at least one homogeneous direction*

As an example we consider a channel flow with the y-axis along the wall-normal direction and periodic boundary conditions in the x- and z-directions. Since the flow is homogeneous in the (x,z)-plane, we impose the constraint that C can depend only on time and the y-coordinate. It is necessary to assume (as did Germano *et al.*) that the filtering kernel $G(\boldsymbol{x},\boldsymbol{y})$ is defined so as to be independent of the cross-channel direction, y. Such an assumption would strictly hold if the grid in the y-direction was sufficiently fine that the flow would be completely resolved in the y-direction. Usually this is not the case, so such an assumption is not justifiable. However, if one does make this assumption the formulas used by the previous authors can be rigorously derived from the variational formulation. Thus, since the filtering is only in x and z and C is assumed independent of x and z, C may be taken out of the filtering operation so that the functional (2.2) reduces to

$$\mathscr{F}[C] = \int \mathrm{d}y \langle (\mathscr{L}_{ij} - m_{ij}C)(\mathscr{L}_{ij} - m_{ij}C)\rangle_{xz} \tag{3.3}$$

where $\langle\ \ \rangle_{xz}$ denotes integral over the (x,z)-plane. The condition for an extremal of the functional (3.3) may be written as

$$\delta\mathscr{F} = 2\int \mathrm{d}y\, \delta C(y)\langle m_{kl}m_{kl}C - m_{ij}\mathscr{L}_{ij}\rangle_{xz} = 0 \tag{3.4}$$

which implies

$$\langle m_{ij}\mathscr{L}_{ij} - m_{kl}m_{kl}C\rangle_{xz} = 0, \tag{3.5}$$

and since C is independent of x and z and m_{ij} is without trace,

$$C(y,t) = \frac{\langle m_{ij}L_{ij}\rangle_{xz}}{\langle m_{kl}m_{kl}\rangle_{xz}}. \tag{3.6}$$

This is the same expression as that of Germano *et al.* and Lilly for flows homogeneous in the (x,z)-plane.

In practice, situations may arise where the C computed using (3.6) is still negative at some points even after averaging over the homogeneous directions. This may happen for example when the number of points in the homogeneous direction or plane is too small to ensure a statistically significant sample. In such situations practitioners (e.g. Zang *et al.* 1993) have sometimes resorted to a 'clipping' scheme, that is taking only the positive part of (3.6). The present formulation allows for a rigorous reinterpretation for this seemingly arbitrary procedure. If one imposes the constraints $C = C(y,t)$ and $C \geqslant 0$ and also assumes $G(\boldsymbol{x},\boldsymbol{y})$ to be independent of the cross-channel direction then the problem reduces to minimizing (3.3) subject to the

constraint $C \geqslant 0$. It can be readily verified (using the method presented in the next section) that the solution to this constrained variational problem is

$$C(y,t) = \left[\frac{\langle m_{ij}L_{ij}\rangle_{xz}}{\langle m_{kl}m_{kl}\rangle_{xz}}\right]_+ \tag{3.7}$$

where the operation of taking the positive part, denoted by the suffix '+', is defined as $x_+ = \frac{1}{2}(x + |x|)$ for any real number x.

3.3. *Inhomogeneous flows*

In this section we will insist that the eddy viscosity be positive and defer the issue of backscatter to §4. Accordingly, in the problem of minimizing the functional in (2.2), we impose the constraint

$$C \geqslant 0. \tag{3.8}$$

It is convenient to write the variational problem in terms of a new variable ξ such that $C = \xi^2$. Then the constraint (3.8) is equivalent to the condition that ξ be real. In terms of the new variable ξ, (2.5) becomes

$$\int \left(-\alpha_{ij}E_{ij} + \beta_{ij}\int E_{ij}(\boldsymbol{y})G(\boldsymbol{y},\boldsymbol{x})\mathrm{d}\boldsymbol{y}\right)\xi(\boldsymbol{x})\delta\xi(\boldsymbol{x})\,\mathrm{d}\boldsymbol{x} = 0, \tag{3.9}$$

which gives for the Euler–Lagrange equation

$$\left(-\alpha_{ij}E_{ij} + \beta_{ij}\int E_{ij}(\boldsymbol{y})G(\boldsymbol{y},\boldsymbol{x})d\boldsymbol{y}\right)\xi(\boldsymbol{x}) = 0. \tag{3.10}$$

Therefore, at any point $\boldsymbol{x}$, either $\xi(\boldsymbol{x}) = 0$ or the first factor in (3.10) vanishes. That is, at some points of the field $C(\boldsymbol{x}) = 0$ and at the remaining points

$$C(\boldsymbol{x}) = \mathscr{G}[C(\boldsymbol{x})]$$

where

$$\mathscr{G}[C(\boldsymbol{x})] = f(\boldsymbol{x}) + \int \mathscr{K}(\boldsymbol{x},\boldsymbol{y})C(\boldsymbol{y})\mathrm{d}\boldsymbol{y}$$

with $f(\boldsymbol{x})$ and $\mathscr{K}(\boldsymbol{x},\boldsymbol{y})$ as defined in §2. Note however, we do not know in advance in which part of the domain C vanishes; this information is part of the solution of the variational problem. C can be found using the following iteration scheme:

$$C_{n+1}(\boldsymbol{x}) = \begin{cases} \mathscr{G}[C_n(\boldsymbol{x})], & \text{if } \mathscr{G}[C_n(\boldsymbol{x})] \geqslant 0; \\ 0, & \text{otherwise.} \end{cases} \tag{3.11}$$

If the iteration process converges then the solution may be written concisely as

$$C(\boldsymbol{x}) = \left[f(\boldsymbol{x}) + \int \mathscr{K}(\boldsymbol{x},\boldsymbol{y})C(\boldsymbol{y})\mathrm{d}\boldsymbol{y}\right]_+ \tag{3.12}$$

where + denotes the positive part. It is clear that a solution of (3.12) satisfies the Euler–Lagrange equation (3.10), but it is not obvious whether this solution is unique (we exclude the trivial solution $C(\boldsymbol{x}) = 0$). Equation (3.10) is a nonlinear integral equation and no rigorous results regarding the existence or uniqueness of its solutions are known to the authors, though numerical experiments indicate that it does have a unique non-trivial solution for all cases studied so far.

The Euler–Lagrange equation (3.12) (or (2.7)) only ensures that the solution is an extremum or a saddle point of the functional. However, it is simple to show that in

the case of the unconstrained problem (2.7) actually represents a minimum. From (2.2) we have (for perturbations in C that are not necessarily small)

$$\delta\mathscr{F} = 2\int E_{ij}(\boldsymbol{x})\delta E_{ij}(\boldsymbol{x})\,\mathrm{d}\boldsymbol{x} + \int \delta E_{ij}(\boldsymbol{x})\delta E_{ij}(\boldsymbol{x})\,\mathrm{d}\boldsymbol{x}. \tag{3.13}$$

The first term vanishes if $C(\boldsymbol{x})$ satisfies (2.7), so that $\delta\mathscr{F} \geqslant 0$. Therefore, we have a minimum of $\mathscr{F}[C]$. We have not been able to carry out the proof for the constrained problem. However, there seems to be some numerical evidence that the stationary solution (3.12) of the variational problem is indeed a minimum (D. Carati, private communication).

The solution of (3.12) gives a fully space–time-dependent coefficient field C which shares all the desirable features of the original dynamic model of Germano *et al.* It vanishes when the flow is laminar, it yields the 'y^3-law' for the eddy viscosity near the wall and it is self-calibrating. However, in contrast to the original formulation of Germano *et al.* this model is applicable to fully inhomogeneous flows where it is intrinsically stable by virtue of the non-negativeness of the eddy viscosity. In this sense it is a generalization of the original dynamic model to inhomogeneous flows. Some examples of its application will be provided in §6.

4. A model involving the subgrid-scale kinetic energy

4.1. *Motivation*

The stability problem associated with the Smagorinsky model with the (unconstrained) variational determination of the coefficient can be understood in the following way. The Smagorinsky model (1.1) does not contain any information regarding the total amount of energy in the subgrid scales. Therefore, if the coefficient C becomes negative in any part of the domain, the model does not have any information on the available energy in the subgrid scales and is therefore unable to provide a mechanism to saturate the reverse flow of energy. However, in a physical system, if all the energy available in the subgrid scales is removed the subgrid-scale stress will go to zero, thus quenching the reverse flow of energy. Clearly, a more elaborate model that keeps track of the subgrid-scale kinetic energy is required. Such a model is described in §4.2. There we allow C to have either sign but make the eddy viscosity depend on the subgrid-scale kinetic energy k. When this is coupled with a transport equation for k, the method allows backscatter, without any instability. The energy flows back and forth between the resolved and subgrid scales while their sum decays monotonically due to viscous effects in the absence of external input of energy.

It should be noted that even though the model we present here is a workable model that does describe the reverse flow of energy from the subgrid to resolved scales, the mechanism, representation as well as importance of backscatter is a matter of some contention among researchers. Intuitively one can think of the energy transfer as arising due to the effect of the very small-scale eddies acting on the resolved scales across a 'spectral-gap' together with another term that represents the effect of the intermediate-size eddies that constitute the 'spectral-gap'. The first contribution can be very well approximated by a (positive) eddy viscosity if the spectral gap is sufficiently large. On the other hand there is no reason to believe that the effect of the intermediate-size eddies can be represented by a gradient diffusion model. It is these intermediate-size eddies that are thought to be responsible for the phenomenon of backscatter. Some models have been suggested that represent the effect of these intermediate eddies as a stochastic force added to the eddy viscosity term. Chasnov

(1990, 1991) extensively studied the influence of this 'eddy forcing' in LES of isotropic turbulence within the framework of the EDQNM approximation. The influence of adding a stochastic term has also been explored in the context of boundary layers (Mason & Thomson 1992) and plane mixing layers (Leith 1990). These authors claim that the inclusion of such a random backscatter improves the agreement of the simulation with experiments. From a theoretical point of view however, this stochastic model of backscatter may be just as unsatisfactory as the gradient diffusion model. Modelling backscatter as a stochastic noise totally uncorrelated from one time-step to the next implies that the correlation time of the intermediate eddies is much shorter than that of the smallest resolved eddies. This is clearly not the case since the smallest resolved eddies are not much larger than the intermediate ones. The interpretation of 'backscatter' is also subject to considerable uncertainities since the intensity of backscatter is found to depend strongly on the filter type (Piomelli *et al.* 1991). These issues will have to be better understood before any meaningful assessment of the importance of backscatter in LES and the best way to represent it can be achieved. The question of backscatter is discussed in some detail in a forthcoming paper (Carati, Ghosal & Moin 1995).

4.2. *The model*

From dimensional analysis, the turbulent viscosity is the product of a velocity and a length scale. We will take the square root of the subgrid-scale kinetic energy† for a velocity scale and the filter width as a length scale. Thus,

$$\tau_{ij} - \tfrac{1}{3}\delta_{ij}\tau_{kk} = -2C\Delta k^{1/2}\overline{S}_{ij} \tag{4.1}$$

and

$$T_{ij} - \tfrac{1}{3}\delta_{ij}T_{kk} = -2C\widehat{\Delta}K^{1/2}\widehat{\overline{S}}_{ij} \tag{4.2}$$

where

$$k = \tfrac{1}{2}(\overline{u_i u_i} - \overline{u}_i\overline{u}_i) = \tfrac{1}{2}\tau_{ii}, \tag{4.3}$$

$$K = \tfrac{1}{2}(\widehat{\overline{u_i u_i}} - \widehat{\overline{u}}_i\widehat{\overline{u}}_i) = \tfrac{1}{2}T_{ii}. \tag{4.4}$$

On taking the trace of (1.5) and using (4.3) and (4.4) we have‡

$$K = \widehat{k} + \tfrac{1}{2}L_{ii}. \tag{4.5}$$

On substituting (4.1) and (4.2) into (1.5) and solving the corresponding variational problem we get (2.7) with $\alpha_{ij} = -2\widehat{\Delta}K^{1/2}\widehat{\overline{S}}_{ij}$ and $\beta_{ij} = -2\Delta k^{1/2}\overline{S}_{ij}$ to determine $C(\boldsymbol{x})$.

To complete the model, it remains to give a method for determining k. For this

† The possibility of treating the dynamic model in conjunction with an equation for turbulent kinetic energy was considered by Wong (1992) in a different context.

‡ If $G(\boldsymbol{x},\boldsymbol{y}) \geqslant 0$ then k, K and L_{ii} are always non-negative. This follows from writing the expression for k, K or L_{ii} in discrete form and using the inequality $\left(\sum_i w_i X_i\right)^2 \leqslant \left(\sum_i w_i\right)\left(\sum_i w_i X_i^2\right)$ where the sum of the weights w_i is unity. The inequality is obtained by putting $\boldsymbol{a} = (w_1^{1/2}, w_2^{1/2}, w_3^{1/2})$ and $\boldsymbol{b} = (w_1^{1/2}X_1, w_2^{1/2}X_2, w_3^{1/2}X_3)$ in Cauchy-Schwarz inequality $|\boldsymbol{a}\cdot\boldsymbol{b}| \leqslant \|\boldsymbol{a}\|\cdot\|\boldsymbol{b}\|$. Note however that the result is not true for the Fourier cut-off filter where $G(\boldsymbol{x},\boldsymbol{y})$ assumes negative values so that some of the weights w_i may be negative. Therefore, in this paper a non-negative filter is always implied.

we will use the well known model of the transport equation for k (see for example, Speziale 1991)

$$\partial_t k + \bar{u}_j \partial_j k = -\tau_{ij}\bar{S}_{ij} - C_* \frac{k^{3/2}}{\Delta} + \partial_j(D\Delta k^{1/2}\partial_j k) + Re^{-1}\partial_{jj}k \tag{4.6}$$

with the grid spacing Δ taken as the length scale appropriate for the subgrid-scale eddies. Here C_* and D are non-negative dimensionless functions of position and time, Re is the Reynolds number and τ_{ij} is given by (4.1). The coefficients C_* and D can be determined dynamically (see the Appendix):

$$C_*(x) = \left[f_*(x) + \int \mathscr{K}_*(x,y) C_*(y) \mathrm{d}y \right]_+ \tag{4.7}$$

and

$$D(x) = \left[f_D(x) + \int \mathscr{K}_D(x,y) D(y) \mathrm{d}y \right]_+ . \tag{4.8}$$

4.3. *Stability*

First it will be shown that the model described in §4.2 is globally stable, that is, the total energy in the large-eddy field remains bounded in the absence of external forces and with boundary conditions consistent with no influx of energy from the boundaries. Using the continuity and momentum equations for the large-eddy fields and (4.6) we derive an equation for the total energy in the resolved as well as the subgrid scales:

$$\frac{\mathrm{d}}{\mathrm{d}t}\left(\frac{1}{2}\int \bar{u}_i \bar{u}_i \mathrm{d}V + \int k \mathrm{d}V \right) = -\int \frac{C_*}{\Delta} k^{3/2} \mathrm{d}V - Re^{-1} \int (\partial_j \bar{u}_i)(\partial_j \bar{u}_i) \mathrm{d}V. \tag{4.9}$$

Here the integral is over the region occupied by the fluid. Boundary conditions are assumed to be such that there is no net flux of energy from the boundaries of the domain so that the surface terms vanish. Note that the terms in $\tau_{ij}\bar{S}_{ij}$ which appear as a source term for k and a sink for the resolved scales (if $C > 0$ and vice versa when $C < 0$) have cancelled out in (4.9) and we are left with the result that in the absence of externally imposed forces and non-trivial boundary conditions the total energy in the large and small scales taken together must monotonically decrease as a result of molecular viscosity. Using the notation

$$E(t) = \frac{1}{2}\int \bar{u}_i \bar{u}_i \mathrm{d}V \tag{4.10}$$

and

$$e(t) = \int k \mathrm{d}V \tag{4.11}$$

we have by (4.9), $E(t)+e(t) \leqslant E(0)+e(0)$ and since $e(t) \geqslant 0$ (see §4.4), $E(t) \leqslant E(0)+e(0)$. Thus, the energy in the large-eddy field cannot diverge even though the eddy viscosity is allowed to be negative.

4.4. *Realizability*

It is necessary to demonstrate that the k computed using (4.6) has the following property: $k(x,t) \geqslant 0$ at all points x at all times t if $k(x,0) \geqslant 0$. This condition is required because it is clear from its definition that k cannot be negative and indeed the model described in §4.2 cannot be implemented unless the non-negativeness of k

can be guaranteed. This condition is part of and included in a more general condition of 'realizability' required of subgrid-scale models (Schumann 1977; Lumley 1978).

Suppose that initially ($t = 0$), $k > 0$ at all points. Let $t = t_0$ be the earliest time for which k becomes zero at some point in the domain. Let this point be $\boldsymbol{x} = \boldsymbol{x}_0$. It will be shown that $\partial_t k(\boldsymbol{x}_0, t_0) > 0$ which ensures that k can never decrease below zero. Integration of (4.6) over an infinitesimal sphere of radius ϵ centred around $\boldsymbol{x}_0$ gives after dividing by ϵ^3

$$\frac{\partial k}{\partial t} = -\frac{1}{\epsilon^3}\int \bar{u}_n k \mathrm{d}\sigma + C\Delta k^{1/2}|\bar{S}|^2 - \frac{C_*}{\Delta}k^{3/2} + \frac{1}{\epsilon^3}\int \nu \frac{\partial k}{\partial n}\mathrm{d}\sigma, \tag{4.12}$$

where $\nu = Re^{-1} + D\Delta k^{1/2}$ and $\mathrm{d}\sigma$ is an infinitesimal element of area on the surface of the sphere. Since $k = \nabla k = 0$ at '$\boldsymbol{x}_0$', $k \sim \epsilon^2$ and $\nabla k \sim \epsilon$ inside the sphere. Therefore, each term on the right side of (4.12) is of order ϵ or higher except for the last term which is of order one. On taking the limit $\epsilon \to 0$ in (4.12) we have

$$\frac{\partial k}{\partial t} = Re^{-1} \lim_{\epsilon \to 0} \frac{1}{\epsilon^3}\int \frac{\partial k}{\partial n}\mathrm{d}\sigma. \tag{4.13}$$

Since k is a minimum at the point $\boldsymbol{x}_0$, the right-hand side is positive. Therefore k can never decrease below zero. Note that we have assumed C, C_* and D remain finite as $k \to 0$. This is true since from (4.5) K remains finite as $k \to 0$ so that the denominators in the integral equations for C, C_* and D do not vanish in this limit. Also, in this proof we assumed that the 'surface' $k = k(\boldsymbol{x}, t_0)$ has only a first order contact with the $k = 0$ surface, that is, the second derivatives of k at $\boldsymbol{x}_0$ are not all zero. The proof however can be easily extended to the general case – one only needs to replace '$k \sim \epsilon^2$' by '$k \sim \epsilon^m$' in the above argument where m is the order of the lowest non-zero derivative of k.

The requirement that k be non-negative is contained in a more general set of properties of the tensor τ_{ij}. They are called realizability conditions and may be stated in several equivalent forms (Schumann 1977). Since the subgrid stress τ_{ij} is a real symmetric tensor, it can be diagonalized where the diagonal elements τ_α, τ_β and τ_γ are real. The realizability conditions can be stated as

$$\tau_\alpha, \tau_\beta, \tau_\gamma \geqslant 0. \tag{4.14}$$

It will be noted that (4.14) implies

$$k = \tfrac{1}{2}\tau_{ii} = \tfrac{1}{2}(\tau_\alpha + \tau_\beta + \tau_\gamma) \geqslant 0. \tag{4.15}$$

Positivity of the turbulent kinetic energy is therefore a consequence of the more general conditions (4.14).

The modelled subgrid-scale stress (4.1) is diagonal in a coordinate system aligned with the principal axes of the rate of strain tensor and the diagonal elements are

$$\tau_i = -2C\Delta k^{1/2} s_i + \tfrac{2}{3}k \tag{4.16}$$

where s_i ($i = \alpha, \beta, \gamma$) are eigenvalues of the rate of strain. The realizability conditions (4.14) are therefore equivalent to the condition

$$C_{min} = -\frac{k^{1/2}}{3\Delta|s_\gamma|} \leqslant C \leqslant \frac{k^{1/2}}{3\Delta s_\alpha} = C_{max} \tag{4.17}$$

at each point of the field. In (4.17) the eigenvalues of the strain rate tensor have been arranged so that $s_\alpha \geqslant s_\beta \geqslant s_\gamma$. The incompressibility condition implies $s_\alpha + s_\beta + s_\gamma = 0$

and therefore $s_\alpha \geqslant 0$, $s_\gamma \leqslant 0$ and s_β may be of either sign. Since C is obtained by solving the integral equation (2.7), it is difficult to prove any general mathematical result on whether the realizability condition (4.17) is satisfied. It is found from numerical experiments on LES of freely decaying isotropic turbulence (§6) that the condition (4.17) is not strictly satisfied. However, the proportion of points falling inside the range $C_{min} \leqslant C \leqslant C_{max}$ exceeds 95%. Thus, the model ensures that $k \geqslant 0$ but is not strictly realizable in the stronger sense of guaranteeing the positivity of the eigenvalues of the subgrid stress.

4.5. *Galilean invariance*

The Navier–Stokes equations are invariant with respect to the transformations

$$x_i' = x_i - Ut, \tag{4.18}$$

$$t' = t, \tag{4.19}$$

$$u_i' = u_i - U \tag{4.20}$$

where U is independent of space and time. It will be shown that the model described in this section as well as the constrained variational formulation of §3 lead to Galilean invariant equations for the large-eddy field.

Substituting (4.20) in the definition of the Leonard term we derive $L_{ij}' = L_{ij}$. Since U is constant clearly the rate of strain tensors are invariant. It is shown in the Appendix that (4.6) for the subgrid-scale kinetic energy is Galilean invariant. Therefore, $k' = k$ and on using (4.5), $K' = K$. Therefore, each term in the integral equation (3.12) in the constrained variational formulation and in (2.7) in the subgrid-scale kinetic energy formulation are invariant, so that $C' = C$. The invariance of the model now follows on using $\partial/\partial x_i' = \partial/\partial x_i$ and $\mathrm{D}/\mathrm{D}t' = \mathrm{D}/\mathrm{D}t$.

4.6. *Behaviour near solid walls*

Consider a point near the wall with x, y and z in the streamwise, wall-normal and spanwise directions respectively. Then near the wall $\overline{u}_1$, $\widehat{\overline{u}}_1$, $\overline{u}_3$, $\widehat{\overline{u}}_3 \sim y$ and hence, by the continuity equation, $\overline{u}_2$, $\widehat{\overline{u}}_2 \sim y^2$ (see e.g. White 1974). From its definition $k = \overline{u_i u_i} - \overline{u}_i \overline{u}_i$ we must have $k \sim y^2$. In order to obtain such a behaviour from (4.6) one needs to impose the boundary conditions that both k and $\partial_y k$ vanish at the walls. However, since (4.6) is only second order in space, we cannot impose both these conditions. Thus, we are forced to choose only $k = 0$ at the wall and this in general will give a solution with the asymptotic behaviour $k \sim y$†. One possible remedy is to consider a two-equation model (such as a k-ϵ model) in place of (4.6). This gives a system that is fourth order in spatial derivatives and can therefore support the additional boundary condition (Durbin 1990). In this paper however we restrict ourselves to the simpler one-equation model (4.6) and therefore the k obtained by solving (4.6) will in general have the behaviour $k \sim y$. Nevertheless we will show that with the model coefficients computed dynamically, the eddy viscosity is proportional to y^3 and the molecular diffusion of kinetic energy balances the viscous dissipation near the wall independent of whether $k \sim y$ or $k \sim y^2$. To stress this generality we will write $k \sim y^{2m}$ where $m = \frac{1}{2}$ or 1.

† Dr W. H. Cabot (private communication) has observed a $k \sim y^2$ near-wall behaviour in channel flow even though only the boundary condition $k = 0$ is imposed. It is possible that the correct near-wall behaviour is somehow embedded in the equations themselves even though it is not explicitly enforced through the boundary conditions.

The strain rate is dominated by the components $\overline{S}_{12}$ and $\widehat{\overline{S}}_{12}$ which are finite and non-zero at the wall. The trace of the Leonard term $L_{ii} \sim y^2$, hence by (4.5) $K \sim y^{2m}$. Thus $\alpha_{12} \sim \beta_{12} \sim y^m$ are the only surviving terms of α_{ij} and β_{ij} near the wall. With these estimates $\mathscr{K}(\boldsymbol{x}, \boldsymbol{y}) \sim 1$ so that from (2.7)

$$C(\boldsymbol{x}) \sim f(\boldsymbol{x}) \sim \frac{L_{12}}{\alpha_{12}} = -\frac{L_{12}}{2\Delta k^{1/2}\overline{S}_{12}}.$$

Thus, the eddy viscosity $\nu_t = C\Delta k^{1/2} \sim L_{12} = \widehat{\overline{u}_1\overline{u}_2} - \widehat{\overline{u}}_1\widehat{\overline{u}}_2 \sim y^3$, the well known '$y^3$-law of the wall'.

We now consider the balance of terms in the k-equation (4.6) in the vicinity of the wall. Using the estimates given in the previous paragraph, it is easily shown from the expressions presented in the Appendix that $\mathscr{K}_D \sim 1$, so that $D \sim f_D$ at the wall. If we expand the pressure near the wall as $p = p_0 + yp_1 + \cdots$ and note that close to the wall the only significant variation of any quantity is in the wall-normal direction, we obtain from (A 4) in the Appendix $Z_1 \sim yu_1 \sim y^2$, $Z_2 \sim yu_2 \sim y^3$, $Z_3 \sim yu_3 \sim y^2$. The only surviving components of $\boldsymbol{X}$ and $\boldsymbol{Y}$ near the wall are $X_2 \sim Y_2 \sim \Delta y^{3m-1}$. Therefore, $f_D \sim Z_2/X_2 \sim y^{4-3m}/\Delta$ so that $D\Delta k^{1/2} \sim y^{4-2m} \to 0$ at the wall. On using the expressions for $\mathscr{K}_*$ and f_* given in the Appendix it is again easily verified that near the wall $\mathscr{K}_* \sim 1$ and hence

$$C_* k^{3/2} \sim f_* k^{3/2} \sim |\Delta Re^{-1}\partial_{jj}L_{ii}|$$

which is finite. Hence,

$$\frac{C_* k^{3/2}/\Delta}{|Re^{-1}\partial_{jj}k|} \sim 1$$

independent of Δ and Re. The remaining terms in the k-equation clearly vanish near the wall. Thus, all terms in the kinetic energy equation go to zero at the wall except the viscous dissipation and diffusion terms. These are finite and are of comparable magnitude at any Reynolds number and grid resolution. This is the correct near-wall behaviour of the turbulent kinetic energy equation (Mansour, Kim & Moin 1988). It should be noted that the integral equations can be written directly in terms of the variables $C\Delta^2$, $D\Delta$ and C_*/Δ and in this form Δ appears only as the ratio $\widehat{\Delta}/\Delta$. Therefore the nature of variation of Δ near the wall is irrelevant in the above analysis.

4.7. *Transition to turbulence*

In a laminar flow undergoing a transition to turbulence the subgrid-scale kinetic energy must undergo a rapid transition from $k = 0$ to some finite value characteristic of the turbulent state. We attempt to demonstrate that (4.6) does have the appropriate behavior using a simplified analysis. The demonstration is qualitative in nature and does not constitute a rigorous proof.

In a Lagrangian frame moving with the resolved velocity, the equation for the subgrid energy of a fluid parcel can be written from (4.6) and (4.1) as

$$\frac{\mathrm{d}k}{\mathrm{d}t} = C\Delta k^{1/2}|\overline{S}|^2 - C_*\frac{k^{3/2}}{\Delta}. \tag{4.21}$$

We are ignoring the diffusion term for the purpose of this qualitative analysis. Equation (4.21) can be written as

$$\frac{\mathrm{d}k}{\mathrm{d}t} = ak^{1/2} - b^2k^{3/2} \tag{4.22}$$

where $a = C\Delta|\bar{S}|^2$ and $b^2 = C_*/\Delta$ will be assumed constant for simplicity. For $a < 0$ (4.22) has only one stationary solution with non-negative k,

$$k = 0, \tag{4.23}$$

which corresponds to a laminar flow. For $a > 0$ there are two stationary solutions, (4.23) as well as

$$k = k_0 = a/b^2, \tag{4.24}$$

which corresponds to turbulence in local equilibrium with production balancing dissipation. It is readily seen on performing a small-perturbation analysis that the solution $k = 0$ is stable for $a \leqslant 0$ but loses stability to $k = k_0$ if $a > 0$.

Since the coefficient C is determined by the Leonard term, C is vanishingly small in a laminar flow and assumes positive values when the flow transitions to turbulence. Thus, during transition a changes from vanishingly small values to finite positive ones. The above stability analysis shows that under these circumstances the k-equation would leave the $k = 0$ solution which has become unstable for the solution (4.24) representing a turbulent state.

5. Numerical implementation

The simplest iteration scheme for solving the integral equation (2.7) is

$$C_{n+1}(x) = C_n(x) + \lambda \left[f(x) + \int \mathscr{K}(x, y) C_n(y) \mathrm{d}y - C_n(x) \right], \tag{5.1}$$

where λ is a relaxation factor. To solve (3.12) one only needs to replace (5.1) by

$$C_{n+1}(x) = C_n(x) + \lambda \left[\left(f(x) + \int \mathscr{K}(x, y) C_n(y) \mathrm{d}y \right)_+ - C_n(x) \right]. \tag{5.2}$$

Convergence can be acheived provided $|\lambda| \leqslant \lambda_0$ where λ_0 is some positive number. In practice it was found that (5.1) or (5.2) would converge only if λ_0 was very small so that this straightforward point-iteration scheme is too slow for practical computations. The following preconditioning scheme was found to greatly increase the rate of convergence as well as the robustness of the scheme.

The integral equation (2.7) may be written in operator notation as

$$(\mathbf{I} - \mathbf{K})C = f. \tag{5.3}$$

On substituting $\mathbf{K} = \mathbf{E} + (\mathbf{K} - \mathbf{E})$ (where $\mathbf{E}$ is for the moment an arbitrary operator) in (5.3) we obtain

$$C = (\mathbf{I} - \mathbf{E})^{-1} f + (\mathbf{I} - \mathbf{E})^{-1}(\mathbf{K} - \mathbf{E})C. \tag{5.4}$$

If C is replaced by C_{n+1} on the left-hand side and by C_n on the right-hand side we obtain the iteration scheme

$$C_{n+1} = (\mathbf{I} - \mathbf{E})^{-1} f + (\mathbf{I} - \mathbf{E})^{-1}(\mathbf{K} - \mathbf{E})C_n. \tag{5.5}$$

Equation (5.5) reduces to (5.1) if we choose $\mathbf{E}$ such that

$$\mathbf{E}\psi = \frac{\lambda - 1}{\lambda}\psi \tag{5.6}$$

where ψ is an arbitrary function of position. It is well known that the speed of convergence of the scheme (5.5) depends on the eigenvalue spectrum of the operator

$$\mathbf{B} = (\mathbf{I} - \mathbf{E})^{-1}(\mathbf{K} - \mathbf{E}). \tag{5.7}$$

The smaller the maximum modulus of the eigenvalues of **B**, the faster is the convergence. An efficient scheme is therefore obtained by choosing **E** such that '**E** $\approx$ **K**' and yet (**I** − **E**) can be readily inverted. One possible choice is

$$\mathbf{E}\psi(\boldsymbol{x}) = \mu V \mathscr{K}(\boldsymbol{x},\boldsymbol{x})\psi(\boldsymbol{x}) \tag{5.8}$$

where V is the volume of the support of the kernel $\mathscr{K}$ and μ is a positive parameter. The motivation for (5.8) is the following:

$$\mathbf{K}\psi = \int \mathscr{K}(\boldsymbol{x},\boldsymbol{y})\psi(\boldsymbol{y})\mathrm{d}\boldsymbol{y} = \mu(\boldsymbol{x})V\mathscr{K}(\boldsymbol{x},\boldsymbol{x})\psi(\boldsymbol{x}) \tag{5.9}$$

where $\mu(\boldsymbol{x})$ is expected to be a positive quantity of order one. Equation (5.9) is exact. Equation (5.8) is the approximation to **K** obtained on ignoring the position dependence of μ. On substituting (5.8) in (5.5) we obtain after some algebra

$$C_{n+1}(\boldsymbol{x}) = \frac{1}{1-\mu g(\boldsymbol{x})}\left[f(\boldsymbol{x}) + \int \mathscr{K}(\boldsymbol{x},\boldsymbol{y})C_n(\boldsymbol{y})\mathrm{d}\boldsymbol{y} - \mu g(\boldsymbol{x})C_n(\boldsymbol{x})\right] \tag{5.10}$$

where

$$g(\boldsymbol{x}) = \frac{\widehat{\Delta}^3}{\alpha_{mn}(\boldsymbol{x})\alpha_{mn}(\boldsymbol{x})}\left[2\alpha_{ij}(\boldsymbol{x})\beta_{ij}(\boldsymbol{x})G(\boldsymbol{x},\boldsymbol{x}) - \beta_{kl}(\boldsymbol{x})\beta_{kl}(\boldsymbol{x})\int [G(\boldsymbol{z},\boldsymbol{x})]^2\mathrm{d}\boldsymbol{z}\right]. \tag{5.11a}$$

When $G(\boldsymbol{x},\boldsymbol{y})$ is a 'top-hat' filter (that is, $G(\boldsymbol{x},\boldsymbol{y})$ is constant inside the cube of edge $\widehat{\Delta}$ centred at $\boldsymbol{x}$ and zero outside) (5.11*a*) reduces to

$$g(\boldsymbol{x}) = \frac{2\alpha_{ij}(\boldsymbol{x})\beta_{ij}(\boldsymbol{x}) - \beta_{kl}(\boldsymbol{x})\beta_{kl}(\boldsymbol{x})}{\alpha_{mn}(\boldsymbol{x})\alpha_{mn}(\boldsymbol{x})}. \tag{5.11b}$$

If μ is chosen between about 0.2 and 0.5, for the 'top-hat' filter the scheme is found to be convergent for arbitrary velocity fields including fields of random numbers for which the point-iteration scheme (5.1) is extremely slow. The iteration is usually started off by using the C field from the previous time-step as the starting guess except for the first time-step where we take $C = 0$ as the first guess.

The kinetic energy version of the model requires initial conditions for the subgrid-scale kinetic energy. In situations where the initial k is not known, the following method can be used to obtain a rough estimate for it from the 'test-window'. If the turbulence is locally at equilibrium, production of turbulent energy equals its dissipation. Under those circumstances one can estimate the subgrid energy as $k \approx 2C_k\Delta^2|\overline{S}|^2$ where C_k is a dimensionless coefficient of order one. Similarly, at the test level, $K \approx 2C_k\widehat{\Delta}^2|\widehat{\overline{S}}|^2$. Substitute these in (4.5) and integrate over the volume of the fluid. Then, on treating C_k as a constant we get

$$C_k = \frac{\langle L_{ii}\rangle}{4\langle\widehat{\Delta}^2|\widehat{\overline{S}}|^2 - \Delta^2\widehat{|\overline{S}|^2}\rangle}. \tag{5.12}$$

In steady-state calculations one can simply take $k = 0$ at the initial time. The solution 'recovers' and approaches the statistical steady state. In the decaying isotropic turbulence computations presented in the next section the initial k was assumed constant in space with an amplitude that was found by integrating the experimental spectrum.

6. Results

As a first step in application of these models a detailed study was made for the simple case of isotropic turbulence. The simplicity of this flow makes it possible to test a subgrid-scale model at a much greater depth than would be possible with a more expensive complex geometry flow. Details of this computation are discussed elsewhere (Carati *et al.* 1995), here we summarize the principal results.

The dynamic localization model (constrained) was then applied to the flow over a backward-facing step. This flow is not fully inhomogeneous; it is still homogeneous in the spanwise direction. However, it has enough of the characteristics of inhomogeneous flows (such as rigid walls, separation, adverse pressure gradient, boundary layer recovery) to enable one to draw reasonable conclusions about the performance of the model in complex geometry situations. The details of this project will be given separately (Akselvoll & Moin, in preparation); here the principal results are summarized. (See also the papers by Le & Moin 1994, Friedrich & Arnal 1990 and Silveira-Neto *et al.* 1993 which are devoted exclusively to the problem of turbulent flow over a backward-facing step.)

6.1. *Isotropic turbulence*

We attempt to simulate the experiment on decaying turbulence behind a grid by Comte-Bellot & Corrsin (1971). The Taylor microscale Reynolds number Re_λ is in the range $71.6 - 60.6$. Turbulence is generated by forcing air through a grid in a wind tunnel and measurements are performed downstream of the grid. In a reference frame moving with the average flow velocity the problem can be thought of as decaying isotropic turbulence. We model this by considering the fluid to be inside a cubical box with periodic boundary conditions. In the experiment, the spectra are measured at three downstream locations. The downstream distance in the experiment is converted to time by using

$$t = \int_0^x \frac{\mathrm{d}x'}{\overline{U}(x')} \tag{6.1}$$

where x is the downstream distance from the grid and $\overline{U}(x)$ is the mean velocity over the cross-section of the wind tunnel. We have non-dimensionalized all experimental data by adopting the length scale $l_*/2\pi$ and the time scale t_* for computational convenience. Here $l_* = 10M$ and $t_* = 64M/U_0$, where $M = 5.08$ cm is the wind tunnel grid spacing and $U_0 = 10^3$ cm s^{-1} is the velocity of the air stream before it impinges on the grid.

Figure 1 shows the energy decay as a function of time computed using the dynamic model (§3.1), dynamic localization model (constrained) (§3.3) and the dynamic localization model (k-equation) (§4) together with the experimental data of Comte-Bellot & Corrsin (1971). The 'resolved' and 'subgrid' energies were obtained by integrating the experimental three-dimensional spectra from $|\boldsymbol{k}| = 0$ to $|\boldsymbol{k}| = 2\pi/\Delta$ and from $|\boldsymbol{k}| = 2\pi/\Delta$ to the maximum wavenumber measured respectively. Here $|\boldsymbol{k}|$ is the magnitude of the wavenumber vector and Δ is the grid spacing. All three models give consistent results that agree well with the experiment. The lower curve is the subgrid-scale kinetic energy (k) as predicted by the k-equation. It is seen to agree quite well with the experiment even though it was computed using only information available at the resolved scale. The dotted line is the result of running the simulation with the model switched off. Clearly the model plays an important role in the successful prediction of the experimental results.

Figure 2 shows the energy spectrum at the initial time and two subsequent times

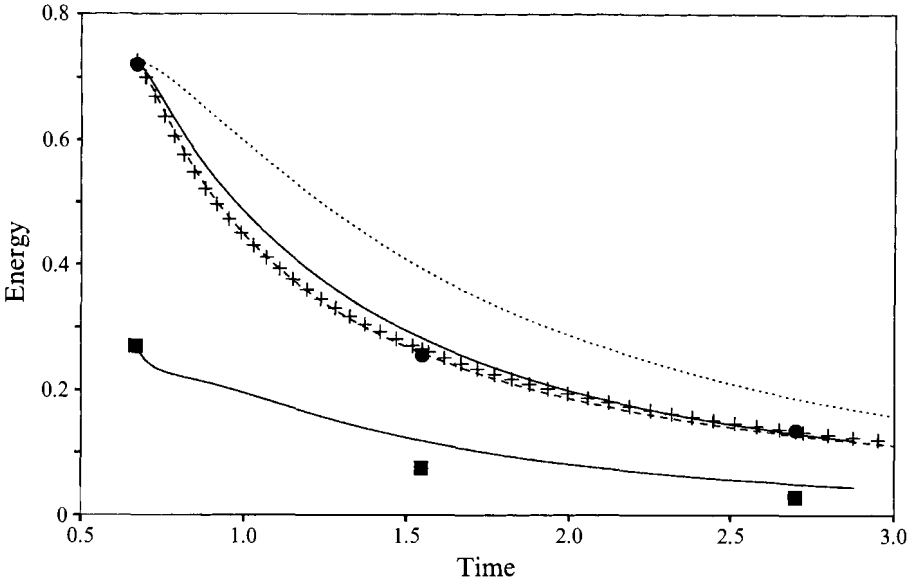

FIGURE 1. Decay of energy in isotropic turbulence: ——— ,dynamic localization model (k-equation) showing resolved (upper curve) and subgrid-scale energy (lower curve); +,dynamic localization model (constrained); — — — , dynamic model; ····· , no model; • , experiment (resolved); ■ , experiment (subgrid). All quantities have been non-dimensionalized by choosing a length scale $l_*/2\pi$ and a time scale t_* where $l_* = 10M$ and $t_* = 64M/U_0$. Here $M = 5.08$ cm is the mesh spacing of the turbulence generating grid and $U_0 = 10^3$ cm s^{-1} is the air speed upstream of the grid

computed using the same three models together with the experimental measurements. The initial velocity field is chosen to match the initial energy spectrum, and the last two curves are the predicted spectra at the same instants of time corresponding to the experimental points in figure 1. The dotted lines are the result of running the simulation with the model switched off. It is seen that in the absence of the model, energy piles up at the high-wavenumber end of the spectrum due to insufficient dissipation. When the model is turned on, it provides just the right amount of dissipation so that the experimental spectra are reproduced.

Figure 3 shows the prediction of the Kolmogorov 5/3 law and Kolmogorov constant for a simulation of forced isotropic turbulence. The external force is defined in the following way in Fourier space. At each time-step an external force

$$\boldsymbol{f}_k = \frac{\epsilon}{N}\frac{\boldsymbol{u}_k}{|\boldsymbol{u}_k|^2} \tag{6.2}$$

is added to the right-hand side of the Navier–Stokes equations for all modes in some chosen wavenumber shell $|\boldsymbol{k}| = k_0$. In (6.2) ϵ is a specified positive number, N is the number of modes in the wavenumber shell and $\boldsymbol{u}_k$ is the velocity vector in wave-space. Clearly, the energy injection rate by the external force is

$$\frac{1}{V}\int \boldsymbol{f}\cdot\boldsymbol{u}\,\mathrm{d}\boldsymbol{x} = \sum \boldsymbol{f}_k\cdot\boldsymbol{u}_k = \epsilon. \tag{6.3}$$

The advantage of this method of forcing is that the energy injection rate is constant in time and is equal to the specified value ϵ. In these simulations we have chosen $k_0 = 2$ and the Reynolds number was taken to be infinite. The energy spectrum was obtained by averaging ten individual spectra, well separated in time, after the

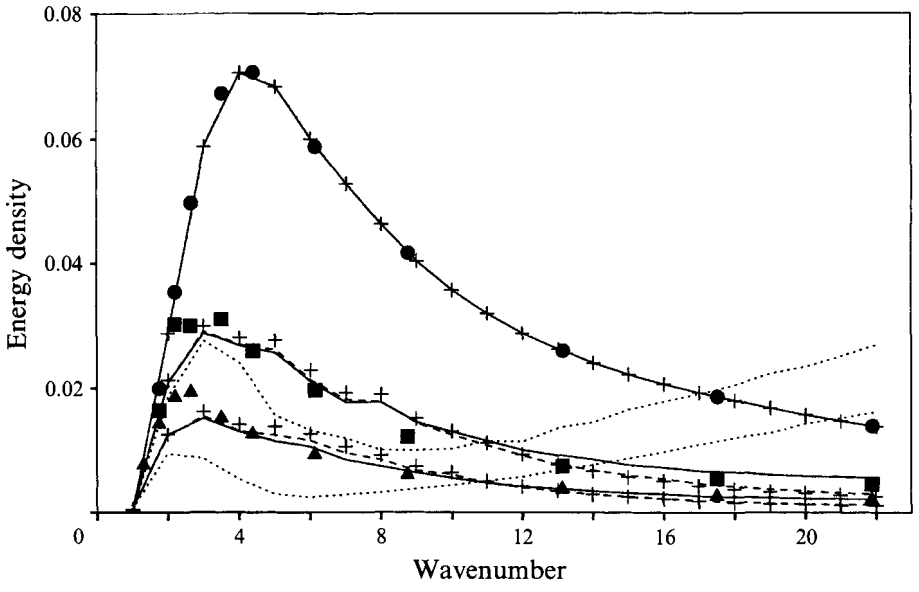

FIGURE 2. Time evolution of spectra in decaying isotropic turbulence: ——— , dynamic localization model (k-equation); +, dynamic localization model (constrained); – – – , dynamic model; ····· , no model; • , experiment (t=0.66); ■ , experiment (t=1.55); ▲ , experiment (t=2.70). All quantities are non-dimensionalized in the same way as in figure 1.

simulation had reached a statistical steady state. The k-equation gives a small plateau in the compensated spectrum $\epsilon^{-2/3}|\boldsymbol{k}|^{5/3}E(|\boldsymbol{k}|)$ corresponding to the 5/3 law and a Kolmogorov constant of $C_\kappa \approx 1.75$. The experimentally measured values of C_κ are in the range 1.3 – 2.1 (Chasnov 1990, 1991), though 1.5 is the commonly accepted value. The dynamic model and the dynamic localization model (constrained) give results that are close to each other but seem to give a somewhat steeper power law spectrum than Kolmogorov's 5/3 law. The best fit seems to be $E(k) \sim k^{-m}$ where $m \approx 2.1$. Since the Reynolds number is infinite the simulation would not reach a steady state if the model is turned off.

It may be of interest to compare the results presented in this section (together with the material in Carati *et al.* mentioned above) with the LES of isotropic flow of Métais & Lesieur (1992). With their so-called 'structure function model' they show that part of the energy spectrum has a 5/3 slope. However, in their theory, the Kolmogorov constant C_k plays the role of an 'adjustable parameter' which is prescribed the value $C_k = 1.4$. The fact that the simulation recovers $C_k \approx 1.4$ is therefore more a test of self-consistency of the model rather than a genuine prediction. By contrast, the value of the Kolmogorov constant reported in this section is a prediction in the sense that assumptions about the value of the Kolmogorov constant have never entered the theory.

In the k-equation version of the dynamic localization model the fraction of points with $C < 0$ was practically constant in time at about 15%. Piomelli *et al.* (1991) find a value of about 40% from DNS data of isotropic turbulence. However, this value was quite sensitive to such details as the choice of the grid filter.

In these computations the iterations for solving the integral equations were carried out until the error in satisfying the integral equation was less than 10% of the r.m.s. value of the corresponding coefficient. Increasing the level of convergence

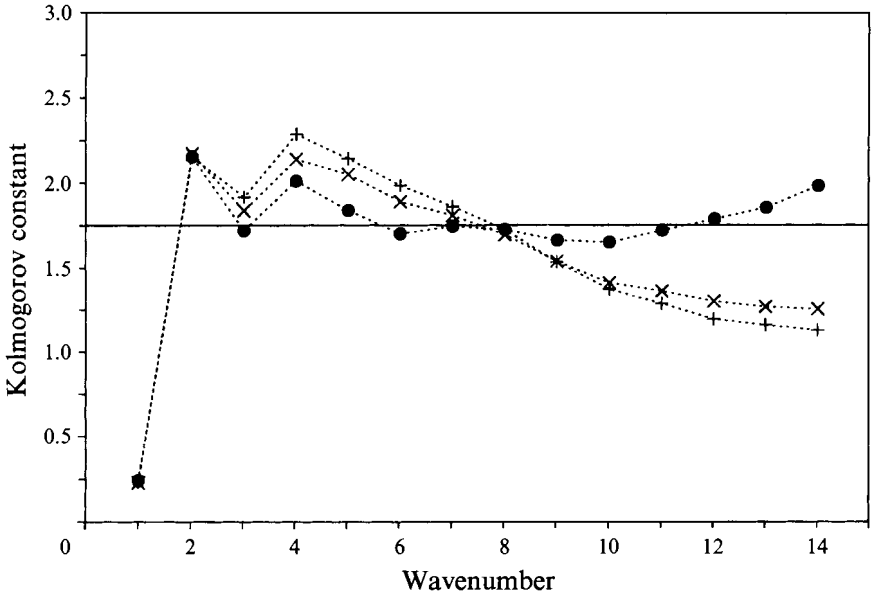

FIGURE 3. Prediction of Kolmogorov's 5/3 law and the Kolmogorov constant in forced isotropic turbulence at steady state: • , dynamic localization model (k-equation); +, dynamic localization model (constrained) ; × , dynamic model.

to machine zero did not have a significant impact on the statistical quantities that were computed. The coefficient fields were evaluated once every time-step using the values at the previous time-step to start the iterations (except at the first time-step where $C = 0$ is used). Under these conditions it was found that the number of iterations required at each time-step typically varied between 4 and 9. Compared to a computation where C was set at a constant value, the dynamic procedure had a CPU overhead of approximately 4%, 16% and 67% for the dynamic model, the dynamic localization model (constrained) and the dynamic localization model (k-equation) respectively. The figures provided here can only serve as a rough indicator of the computational overhead since they will in general depend on the code as well as the computer used.

In isotropic turbulence, the dynamic model as well as the two versions of the dynamic localization model can be consistently derived within the framework of the variational approach. It is therefore not surprising that all three models give comparable results that are in good agreement with the experiments. Further, the effect of the models is very clear in these simulations. If the model is turned off, either agreement with the experiment is very poor (in the decaying case) or a steady state cannot be reached at all (in the forced case).

6.2. *The backward-facing step*

LES has been performed for turbulent flow over a backward-facing step at Reynolds number 28 000 based on the inlet free-stream velocity (U_0) and step height (h). The flow is complex by virtue of the massive separation behind the step, the associated adverse pressure gradient and the recovery downstream of the reattachment region. The LES results are compared with experimental results of Adams, Johnston & Eaton

(1984). The subgrid-scale model used in the calculations is the dynamic localization model (constrained). This model was chosen because it is the simplest one that is still applicable to completely inhomogeneous flows.

The experimental facility used by Adams *et al.* consists of a single-sided expansion with a fixed upper wall. The expansion ratio is 1.25 (upstream channel width is 4 step heights). The flow upstream of the step consists of two developing boundary layers, each of thickness roughly 1.2 step heights. A potential core exists between the boundary layers. An aspect ratio (spanwise extent/step height) of 11.4 was used in order to enhance two-dimensionality of the mean flow in the separated region.

The computational domain starts 10 step heights upstream of the step in order to allow the flow to recover from the inflow boundary condition, and extends 20 step heights downstream of the step. The spanwise extent of the computational domain is 3 step heights. As in the experiment, a solid wall is used at the top boundary. The inflow boundary condition consists of a mean velocity profile with superimposed random fluctuations (Le & Moin 1994). A convective boundary condition is used at the domain exit. In the homogeneous spanwise direction periodic boundary conditions are used and no-slip conditions are employed along all solid walls.

The computational mesh is uniform in the spanwise direction and stretched in both the streamwise and wall-normal directions. Wall-normal stretching of the mesh is necessary in order to resolve the boundary layers. The mesh in the wall-normal direction is designed to resolve the boundary layers upstream as well as downstream of the step. The mesh is also stretched in the streamwise direction, increasing the density of grid points near the corner of the step. This is necessary in order to resolve sharp mean gradients in that region. The computational mesh has $244 \times 96 \times 96$ grid points in the streamwise, wall-normal and spanwise direction, respectively. Based on the friction velocity at the inlet of the domain, the resolution (in wall units) in the streamwise direction is : $\Delta x^+_{min} = 17$ and $\Delta x^+_{max} = 273$. The minimum resolution occurs at the corner of the step. For the wall-normal direction the corresponding numbers are : $\Delta y^+_{min} = 1.8$ and $\Delta y^+_{max} = 227$. The spanwise (uniform) resolution is $\Delta z^+ = 36$. The calculation required about 70 CPU hours on a CRAY-C90. Evaluation of the subgrid-scale model increases the CPU time spent per time-step in the code by about 30%.

An important parameter for comparing the result of the backward-facing step flow is the reattachment location. Adams *et al.* report a reattachment length of 6.7 step heights which is identical to the value calculated in the present simulation. Figure 4 shows the mean streamwise velocity profiles at three locations downstream of the step: $x/h = 4.5$ is in the recirculation region, $x/h = 7.2$ is in the reattachment region and $x/h = 12.2$ is in the recovery region. Overall good agreement between the computation and experiment is observed at all locations. The slight lag of the LES velocity profile compared with the experimental values in the recovery region is believed to be due to the blocking effect of the sidewall boundary layers in the experiment. Figure 5 shows the computed and measured streamwise r.m.s. velocity fluctuation. As with the mean velocity profiles, the overall agreement between the experiment and computation is very good. It should be noted that the simulation results are for the resolvable portion of turbulent intensities whereas the experimental data give the total intensities. The contribution of the subgrid part can be obtained in the k-equation version of the dynamic localization model since the whole of the subgrid stress is represented instead of just the deviatoric part. However, in the present simulation the simpler constrained version of the model was used. Figure 6 compares the result of an LES performed with the dynamic localization model (constrained)

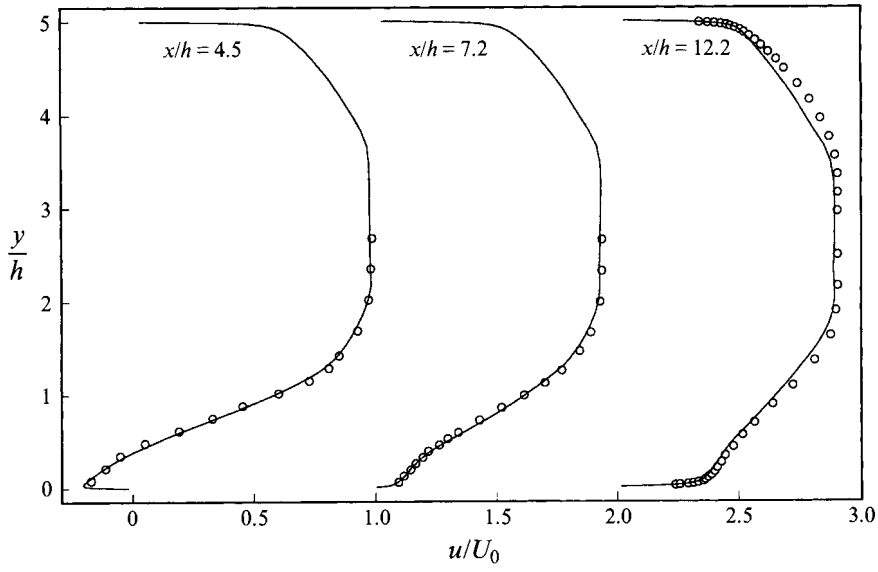

FIGURE 4. Mean streamwise velocity profiles downstream of the step: ——— , LES; o , experimental results of Adams *et al.*

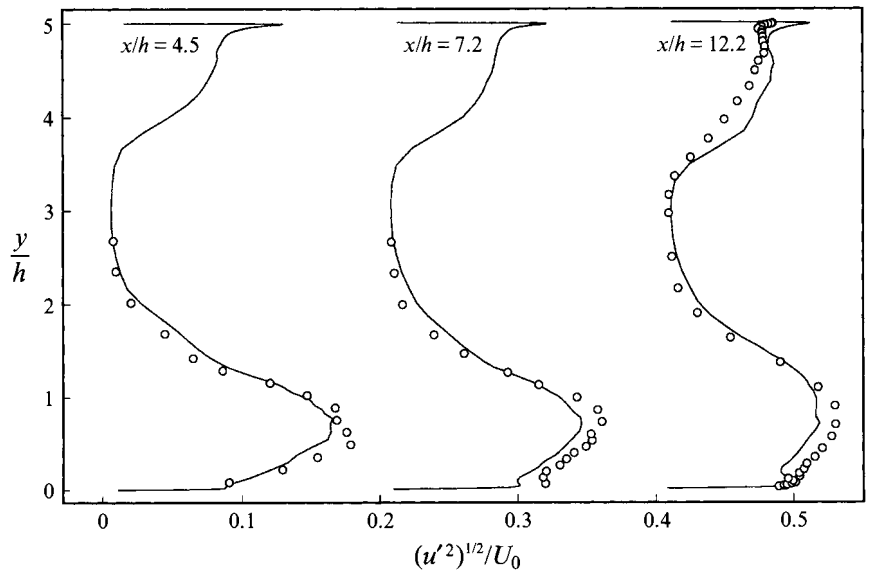

FIGURE 5. Streamwise turbulence velocity fluctuation downstream of the step: ——— , LES; o , experimental results of Adams *et al.*

with that using a 'span averaged and clipped' version similar to (3.7):

$$C(x, y, t) = \left[\frac{\langle m_{ij} L_{ij} \rangle_z}{\langle m_{kl} m_{kl} \rangle_z} \right]_+ . \tag{6.4}$$

It is seen that close to the wall the dynamic localization model (constrained) gives slightly better agreement with the experiment than (6.4). The difference becomes insignificant as one moves further away from the wall.

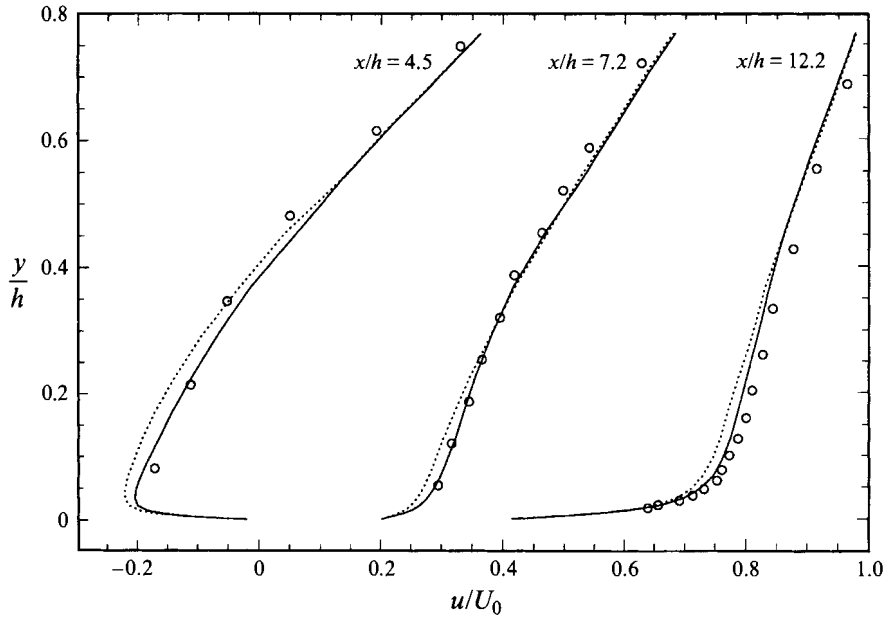

FIGURE 6. Mean streamwise velocity profiles downstream of the step: ——— , LES with dynamic localization model (constrained); ····· , LES with span-averaged and clipped version of the dynamic model; o , experimental results of Adams *et al.*

7. Conclusions

In this paper the solution procedure for obtaining the coefficient in the dynamic model was recast in the context of a variational problem. It was shown that in situations where the flow does have one or more homogeneous directions, the local least-square minimization coupled with the spatial averaging technique used by previous authors may be derived from this variational formulation. Specifically, if one imposes the constraint that C is independent of the homogeneous directions and the test-filtering operation is performed only with respect to the homogeneous directions, the expressions for C used by these previous authors follow as the solution of a constrained variational problem. Under the same conditions if one imposes the additional constraint that $C \geqslant 0$ one derives the prescription where only the positive part of the space-averaged coefficient is taken. These expressions for C have been successfully used in the past in LES but an adequate theoretical justification for using them has been lacking.

The variational formulation allows a generalization of the dynamic procedure to flows that do not necessarily have homogeneous directions. Thus, if $C \geqslant 0$ is chosen as a constraint in the variational problem, an integral equation for determining C is obtained. The integral equation can be solved numerically at each time-step to determine the coefficient field $C(x, y, z, t)$. In this formulation the existence of homogeneous directions in the flow is not required and no restriction need be imposed on the nature of the test filter. We have called this method the dynamic localization model (constrained).

The dynamic localization model (constrained) does not admit backscatter which is known to be a feature of turbulent flows. A subgrid-scale model was constructed using the square root of the turbulent kinetic energy as a velocity scale. This model

has a number of desirable features. In this formulation the restriction that C be non-negative is not imposed. In the absence of external energy input it is shown that the model would necessarily lead to decay of total energy. Thus, the instability of previous formulations due to unregulated backscatter is forbidden by construction. The model is shown to be realizable in the restricted sense of $k \geqslant 0$. That is, the structure of the evolution equations is such that it would never cause the subgrid energy k to assume unphysical negative values. The more general realizability conditions of Schumann are only satisfied in a limited sense (§4.4). Near solid walls the method ensures that the right balance of terms in the k-equation is obtained and that the eddy viscosity goes to zero as the cube of the distance from the wall. This latter property is shared by all the models in the 'dynamic model family' discussed in this paper. An approximate theoretical analysis is presented to show that the k-equation would properly predict a departure from the laminar state $k = 0$ to a turbulent state $k > 0$ when the flow undergoes a transition to turbulence.

Extensive tests have been done on forced as well as freely decaying isotropic turbulence using the dynamic localization model. For isotropic turbulence, both versions of the dynamic localization model as well as the dynamic model give results that are in excellent agreement with experiments. In these tests the effect of the model is quite unambiguous since very poor results are obtained if the simulations are repeated without the model. The dynamic localization model (constrained) is then applied to the backward-facing step flow at a Reynolds number of 28 000. The presence of walls and massive separation make this flow a good test case for evaluating performance of turbulence models in complex geometry flows. The mean streamwise velocity and turbulent intensity are in good agreement with the experiment. The reattachment length is also accurately predicted.

In conclusion, the generality of the dynamic localization model should be emphasized. The basic idea is independent of any particular subgrid-scale model and thus the methods presented here can be used to dynamically determine one or more model coefficients in other subgrid-scale models that might be superior to Smagorinsky's model. There are a number of issues that have to be resolved before the method can be applied to complex flows at high Reynolds numbers. One such issue is the resolution of the wall layers. In order to adequately compute the dynamics near the wall one has to have a dense clustering of grid points in this region so that all flow structures are fully resolved. The dynamic models are very well suited to such situations because when the flow is fully resolved the model automatically drives the eddy viscosity to zero. An efficient way of distributing grid points in a complex flow domain is to use unstructured meshes. The implementation of dynamic models on such unstructured meshes is underway.

This work was supported in part by ONR (under grant N00014-91-J-4072) and AFOSR (under grant F49620-92-J-0003). We would like to thank Dr Nagi Mansour for providing the basic code for isotropic turbulence which we modified to perform the tests described in §6.1. We would also like to thank Dr Daniele Carati for his careful reading of the manuscript and helpful suggestions.

Appendix. The dynamic determination of C_* and D.

The evolution of subgrid-scale kinetic energy is modelled by ((4.6) in the text)

$$\partial_t k + \bar{u}_j \partial_j k = -\tau_{ij}\bar{S}_{ij} - C_*\frac{k^{3/2}}{\Delta} + \partial_j(D\Delta k^{1/2}\partial_j k) + Re^{-1}\partial_{jj}k \qquad \text{(A 1)}$$

where C_* and D ($C_*, D \geqslant 0$) are functions of position and time. By analogy one can write down the corresponding evolution equation for the subtest-scale kinetic energy:

$$\partial_t K + \widehat{\overline{u}}_j \partial_j K = -T_{ij}\widehat{\overline{S}}_{ij} - C_* \frac{K^{3/2}}{\widehat{\Delta}} + \partial_j (D\widehat{\Delta} K^{1/2} \partial_j K) + Re^{-1}\partial_{jj} K. \tag{A 2}$$

Equations (A 1) and (A 2) must be consistent with the relation

$$K = \widehat{k} + \tfrac{1}{2} L_{ii} \tag{A 3}$$

((4.5) in the text). Further, one can derive the following identity relating the flux of subgrid-scale kinetic energy f_j and the corresponding quantity at the test level† F_j:

$$F_j - \widehat{f}_j = Z_j \equiv \widehat{\overline{u}_j \overline{(\overline{p} + k + \overline{u}_i \overline{u}_i/2)}} - \overline{\widehat{u}_j \overline{(\overline{p} + k + \overline{u}_i \overline{u}_i/2)}} \tag{A 4}$$

where $\overline{p}$ is the resolved pressure‡. These facts can be exploited to determine C_* and D as shown below.

To determine D, we substitute the modelled fluxes

$$f_j = D\Delta k^{1/2} \partial_j k \tag{A 5}$$

and

$$F_j = D\widehat{\Delta} K^{1/2} \partial_j K \tag{A 6}$$

into (A 4) to obtain

$$Z_j = X_j D - \widehat{Y_j D} \tag{A 7}$$

where

$$X_j = \widehat{\Delta} K^{1/2} \partial_j K, \tag{A 8}$$

$$Y_j = \Delta k^{1/2} \partial_j k. \tag{A 9}$$

Following the standard methodology, D is obtained on minimizing

$$\int (Z_j - X_j D + \widehat{Y_j D})(Z_j - X_j D + \widehat{Y_j D}) \mathrm{d}\boldsymbol{y} \tag{A 10}$$

subject to the constraint $D \geqslant 0$. The solution to this variational problem can be immediately written down in analogy to the solution (3.12) in the text if one notices the similarity in structure between (A 7) and (1.7):

$$D(\boldsymbol{x}) = \left[f_D(\boldsymbol{x}) + \int \mathscr{K}_D(\boldsymbol{x}, \boldsymbol{y}) D(\boldsymbol{y}) \mathrm{d}\boldsymbol{y} \right]_+ \tag{A 11}$$

where

$$f_D(\boldsymbol{x}) = \frac{1}{X_j(\boldsymbol{x}) X_j(\boldsymbol{x})} \left[X_j(\boldsymbol{x}) Z_j(\boldsymbol{x}) - Y_j(\boldsymbol{x}) \int Z_j(\boldsymbol{y}) G(\boldsymbol{y}, \boldsymbol{x}) \mathrm{d}\boldsymbol{y} \right], \tag{A 12}$$

† We are grateful to Dr W. H. Cabot for bringing this identity to our attention.

‡ There is an analogous identity relating the dissipation at grid level (ϵ_g) and test level (ϵ_t): $\epsilon_t - \widehat{\epsilon_g} = Re^{-1}[\widehat{(\partial_i \overline{u}_j)(\partial_i \overline{u}_j)} - (\partial_i \widehat{\overline{u}}_j)(\partial_i \widehat{\overline{u}}_j)]$. However, this identity is unusable because the right-hand side vanishes at high Reynolds numbers. This is due to the fact that at high Reynolds numbers the molecular dissipation in the inertial range 'test window' is vanishingly small and therefore no estimate of the actual dissipation is possible based on this information.

$$\mathscr{K}_D(x,y) = \frac{\mathscr{K}_{\mathscr{A}}^D(x,y) + \mathscr{K}_{\mathscr{A}}^D(y,x) - \mathscr{K}_{\mathscr{S}}^D(x,y)}{X_j(x)X_j(x)} \tag{A 13}$$

and

$$\mathscr{K}_{\mathscr{A}}^D(x,y) = X_j(x)Y_j(y)G(x,y), \tag{A 14}$$

$$\mathscr{K}_{\mathscr{S}}^D(x,y) = Y_j(x)Y_j(y)\int \mathrm{d}z\, G(z,x)G(z,y). \tag{A 15}$$

To determine C_*, we substitute (A.3) in (A.2) and obtain

$$\partial_t\widehat{k} + \widehat{\overline{u}}_j\partial_j\widehat{k} = -E + \partial_j F_j + Re^{-1}\partial_{jj}\widehat{k} \tag{A 16}$$

where

$$E = T_{ij}\widehat{\overline{S}}_{ij} + \frac{C_*K^{3/2}}{\widehat{\Delta}} - \frac{1}{2}Re^{-1}\partial_{jj}L_{ii} + \frac{1}{2}(\partial_t L_{ii} + \widehat{\overline{u}}_j\partial_j L_{ii}) \tag{A 17}$$

and F_j is given by (A 6). On applying the 'test-filtering' operation to (A 1) we get

$$\partial_t\widehat{k} + \widehat{\overline{u}_j\partial_j k} = -\widehat{\tau_{ij}\overline{S}_{ij}} - \widehat{\frac{C_*k^{3/2}}{\Delta}} + \partial_j\widehat{f}_j + Re^{-1}\partial_{jj}\widehat{k}. \tag{A 18}$$

Now we eliminate $\partial_t\widehat{k}$ between (A 16) and (A 18) and replace the quantity $F_j - \widehat{f}_j$ by its expression (A 4) and T_{ij} by $L_{ij} + \widehat{\tau}_{ij}$ (from the identity (1.5)) to obtain

$$\chi = \phi C_* - \widehat{\psi C_*}. \tag{A 19}$$

Here

$$\chi = \widehat{\tau_{ij}\overline{S}_{ij}} - \widehat{\tau}_{ij}\widehat{\overline{S}}_{ij} - L_{ij}\widehat{\overline{S}}_{ij} + \partial_j\rho_j - \tfrac{1}{2}\mathrm{D}_t L_{ii} + \tfrac{1}{2}Re^{-1}\partial_{jj}L_{ii}, \tag{A 20}$$

$$\phi = K^{3/2}/\widehat{\Delta} \tag{A 21}$$

and

$$\psi = k^{3/2}/\Delta \tag{A 22}$$

where

$$\rho_j = \widehat{\overline{u}_j(\overline{p} + \tfrac{1}{2}\overline{u}_i\overline{u}_i)} - \widehat{\overline{u}_j}\,\widehat{(\overline{p} + \tfrac{1}{2}\overline{u}_i\overline{u}_i)} \tag{A 23}$$

and $\mathrm{D}_t \equiv \partial_t + \widehat{\overline{u}}_j\partial_j$. The subgrid-scale stress τ_{ij} is given by (4.1) in the text so that ϕ, ψ and χ are all computable from the available resolved fields. Since (A 19) is a single integral equation for C_*, one might be tempted to solve it directly without first going through the variational formulation. However, since the viscous dissipation term is necessarily non-negative from its definition, C_* must be non-negative whereas the C_* obtained by solving (A 19) can have either sign. One must therefore try to 'best satisfy' (A 19) subject to the constraint $C_* \geqslant 0$. That is, C_* must be chosen so as to minimize the functional

$$\int (\chi - \phi C_* + \widehat{\psi C_*})^2 \mathrm{d}y$$

with the constraint $C_* \geqslant 0$. Once again the solution to this variational problem can be written down in analogy to (3.12) in the text:

$$C_*(x) = \left[f_*(x) + \int \mathscr{K}_*(x,y)C_*(y)\mathrm{d}y \right]_+ \tag{A 24}$$

where

$$f_*(x) = \frac{1}{\phi^2(x)}\left[\phi(x)\chi(x) - \psi(x)\int \chi(y)G(y,x)\mathrm{d}y\right],$$

$$\mathscr{K}_*(x,y) = \frac{\mathscr{K}_{\mathscr{A}}^*(x,y) + \mathscr{K}_{\mathscr{A}}^*(y,x) - \mathscr{K}_{\mathscr{P}}^*(x,y)}{\phi(x)\phi(x)}$$

and

$$\mathscr{K}_{\mathscr{A}}^*(x,y) = \phi(x)\psi(y)G(x,y),$$

$$\mathscr{K}_{\mathscr{P}}^*(x,y) = \psi(x)\psi(y)\int \mathrm{d}z\, G(z,x)G(z,y).$$

It is readily verified that χ, ϕ, ψ, Z_j, X_j and Y_j are all Galilean invariant. Thus C_* and D obtained by solving (A 11) and (A 24) are also Galilean invariant which in turn impies that the subgrid-scale kinetic energy equation (A 1) itself is Galilean invariant.

REFERENCES

ADAMS, E. W., JOHNSTON, J. P. & EATON, J. K. 1984 Experiments on the structure of turbulent reacting flow. *Rep.* MD-43. Thermosciences Division, Dept of Mech. Engng, Stanford University.

BOHNERT, M. & FERZIGER, J. H. 1993 The dynamic subgrid-scale model in LES of the stratified Eckman layer. In *Engineering Turbulence Modelling and Experiments 2* (ed. W. Rodi & M. Martelli), pp. 315–324. Elsevier.

CABOT, W. H. & MOIN P. 1993 Large-eddy simulation of scalar transport with the dynamic subgrid-scale model. In *Large Eddy Simulation of Complex Engineering and Geophysical Flows* (ed. B. Galperin & S. A. Orszag). Cambridge University Press.

CARATI, D., GHOSAL, S. & MOIN, P. 1995 On the representation of backscatter in dynamic localization models. *Phys. Fluids* (to appear).

CHASNOV, J. R. 1990 Development and application of an improved subgrid model for homogeneous turbulence. PhD thesis, Columbia University.

CHASNOV, J. R. 1991 Simulation of the Kolmogorov inertial subrange using an improved subgrid model. *Phys. Fluids* A **3**, 188–200.

COMTE-BELLOT, G. & CORRSIN, S. 1971 Simple Eulerian time correlation of full and narrow-band velocity signals in grid-generated 'isotropic' turbulence. *J. Fluid Mech.* **48**, 273–337.

DURBIN, P. A. 1990 Near wall turbulence closure modeling without 'damping functions'. *Theor. Comput. Fluid Dyn.* **3**, 1–13.

FRIEDRICH, R. & ARNAL, M. 1990 Analysing turbulent backward-facing step flow with the lowpass-filtered Navier-Stokes equations. *J. Wind Engng Indust. Aerodyn.* **35**, 101–128.

GERMANO, M., PIOMELLI, U., MOIN, P. & CABOT W. 1991 A dynamic subgrid-scale eddy viscosity model. *Phys. Fluids* A **3**, 1760–1765.

LE, H. & MOIN, P. 1994 Direct numerical simulation of flow over a backward-facing step. *Rep.* TF-58. Thermosciences Division, Dept of Mech. Engng, Stanford University.

LEITH, C. E. 1990 Stochastic backscatter in a subgrid-scale model: plane shear mixing layer. *Phys. Fluids* A **2**, 297–299.

LILLY, D. K. 1992 A proposed modification of the Germano subgrid-scale closure method. *Phys. Fluids* A **4**, 633–635.

LUMLEY, J. L. 1978 Computational modeling of turbulent flows. *Adv. Appl. Mech.* **18**, 123–176.

LUND, T. S., GHOSAL, S. & MOIN, P. 1993 Numerical experiments with highly variable eddy viscosity models. In *Engineering Applications of Large Eddy Simulations* (ed. S. A. Ragale & U. Piomelli). FED Vol. 162, pp. 7–11. ASME.

MANSOUR, N. N., KIM, J. & MOIN, P. 1988 Reynolds-stress and dissipation-rate budgets in a turbulent channel flow. *J. Fluid Mech.* **194**, 15–44.

MASON, P. J. & THOMSON, D. J. 1992 Stochastic backscatter in large-eddy simulation of boundary layers. *J. Fluid Mech.* **242**, 51–78.

MÉTAIS, O. & LESIEUR, M. 1992 Spectral large-eddy simulation of isotropic and stably stratified turbulence. *J. Fluid Mech.* **239**, 157–194.

MOIN, P. 1991 A new approach for large eddy simulation of turbulence and scalar transport. In *Proc. Monte Verita Coll. on Turbulence.* Birkhauser, Bale.

MOIN, P., SQUIRES, K., CABOT, W. & LEE, S. 1991 A dynamic subgrid-scale model for compressible turbulence and scalar transport. *Phys. Fluids* A **3**, 2746–2757.

PIOMELLI, U. 1993 High Reynolds number calculations using the dynamic subgrid-scale stress model. *Phys. Fluids* A **5**, 1484–1490.

PIOMELLI, U., CABOT, W. H., MOIN, P. & LEE, S. 1991 Subgrid-scale backscatter in turbulent & transitional flows. *Phys. Fluids* A **3**, 1766–1771.

SCHUMANN, U. 1977 Realizability of Reynolds-stress turbulence models. *Phys. Fluids* **20**, 721–725.

SILVEIRA NETO, A., GRAND, D., MÉTALS, O. & LESIEUR, M. 1993 A numerical investigation of the coherent vortices in turbulence behind a backward-facing step. *J. Fluid. Mech.* **256**, 1–25.

SMAGORINSKY, J. 1963 General circulation experiments with the primitive equations. I. The basic experiment. *Mon. Weather Rev.* **91**, 99–165.

SPEZIALE, C. G. 1991 Analytic methods for the development of reynolds-stress closures in turbulence. *Ann. Rev. Fluid Mech.* **23**, 107–157.

WHITE, F. M. 1974 *Viscous Fluid Flow.* McGraw-Hill.

WONG, V. C. 1992 A proposed statistical-dynamic closure method for the linear or nonlinear subgrid-scale stresses. *Phys. Fluids* A **4**, 1080–1082.

ZANG, Y., STREET, R. L. & KOSEFF, J. R. 1993 A dynamic mixed subgrid-scale model and its application to turbulent recirculating flows. *Phys. Fluids* A **5**, 3186–3196.